Mechanistic and Structural Analysis of Human Spermidine/Spermine N^1-Acetyltransferase[†,‡]

Subray S. Hegde,[§] Jonathan Chandler,[||] Matthew W. Vetting,[§] Michael Yu,[§] and John S. Blanchard*[,§]

Department of Biochemistry, Albert Einstein College of Medicine, 1300 Morris Park Avenue, Bronx, New York 10461, and Pelham Memorial High School, Pelham, New York 10803

Received February 6, 2007; Revised Manuscript Received April 11, 2007

ABSTRACT: The N^1-acetylation of spermidine and spermine by spermidine/spermine acetyltransferase (SSAT) is a crucial step in the regulation of the cellular polyamine levels in eukaryotic cells. Altered polyamine levels are associated with a variety of cancers as well as other diseases, and key enzymes in the polyamine pathway, including SSAT, are being explored as potential therapeutic drug targets. We have expressed and purified human SSAT in *Escherichia coli* and characterized its kinetic and chemical mechanism. Initial velocity and inhibition studies support a random sequential mechanism for the enzyme. The bisubstrate analogue, N^1-spermine−acetyl-coenzyme A, exhibited linear, competitive inhibition against both substrates with a true K_i of 6 nM. The pH−activity profile was bell-shaped, depending on the ionization state of two groups exhibiting apparent pK_a values of 7.27 and 8.87. The three-dimensional crystal structure of SSAT with bound bisubstrate inhibitor was determined at 2.3 Å resolution. The structure of the SSAT−spermine−acetyl-coenzyme A complex suggested that Tyr140 acts as general acid and Glu92, through one or more water molecules, acts as the general base during catalysis. On the basis of kinetic properties, pH dependence, and structural information, we propose an acid/base-assisted reaction catalyzed by SSAT, involving a ternary complex.

The polyamines, spermine, spermidine, and their diamine precursor, putrescine, are naturally occurring polycations that are essential for the normal growth and proliferation of all cells. These ubiquitous molecules play an important role in numerous physiological functions such as cell growth and proliferation, nucleic acid and protein synthesis, cell adhesion and repair of the extracellular matrix, immunity, etc. (*1*−*4* and references cited therein). The cellular concentrations of these compounds are highly regulated via biosynthesis, transport, degradation, and interconversion of these molecules and also through the induction and degradation of the enzymes involved in their biosynthesis and degradation. A reduced level of polyamines has been shown to affect cell proliferation and migration and cause defective embryo development, while overaccumulation induces apoptosis and cell transformation (*4*). Altered levels of polyamines have been found in disease conditions such as Alzheimer's disease (*5*), cystic fibrosis (*6*, *7*), and a variety of tumor and cancer cells (*8*−*12*). The polyamine metabolic pathway in higher mammals, including humans, is well-understood (*2*, *4*, *13* and references cited therein). The first committed and regulatory step in the polyamine biosynthetic pathway is the conversion of ornithine to putrescine by ornithine decarboxylase (Scheme 1). The successive polyamines, spermidine and spermine, are then synthesized by the sequential addition of aminopropyl groups to putrescine catalyzed by their respective synthases (Scheme 1). Spermidine/spermine N^1-acetyltransferase (SSAT), the key enzyme in the catabolism of eukaryotic polyamines, acetylates spermine and spermidine, and the monoacetylated spermidine and spermine are either degraded by N^1-acetylpolyamine oxidase or exported from the cell. The SSAT level is very low under normal conditions and is rapidly induced by a variety of stimuli such as hormones and growth factors, toxic compounds, polyamines and polyamine analogues, certain drugs, and pathophysiological conditions (*14*).

Human SSAT (hSSAT) has previously been purified from cultured melanoma cells, and preliminary kinetic properties have been reported (*15*). The three-dimensional structures of the recombinant hSSAT holoenzyme and a ternary complex have recently been reported (*16*, *17*). In this paper, we report a detailed kinetic and mechanistic characterization, including determining bisubstrate (N^1-spermine-acetyl-CoA) inhibition patterns and the three-dimensional structure of the recombinant hSSAT with a bound bisubstrate inhibitor.

MATERIALS AND METHODS

Materials. All chemicals, coenzyme A derivatives, and polyamines were purchased from Sigma-Aldrich Chemical Co. Enzymes used in molecular biology were supplied by New England Biolabs. Plasmid pET-28a and *Escherichia coli* strains Nova Blue and BL21(DE3) were obtained from Novagen. The *hSSAT* cDNA clone was obtained from Origene Inc.

[†] This work was supported by NIH Grants A1 60899 (to J.S.B.), T32 AI07501 (to M.W.V.), and T32 GM07288 (to M.Y.).

[‡] Structural data have been deposited in the Protein Data Bank (entry 2JEV).

* To whom correspondence should be addressed. Phone: (718) 430-3096. Fax: (718) 430-8565. E-mail: blanchar@aecom.yu.edu.

[§] Albert Einstein College of Medicine.

[||] Pelham Memorial High School.

10.1021/bi700256z CCC: $37.00
Published on Web 05/22/2007

Scheme 1

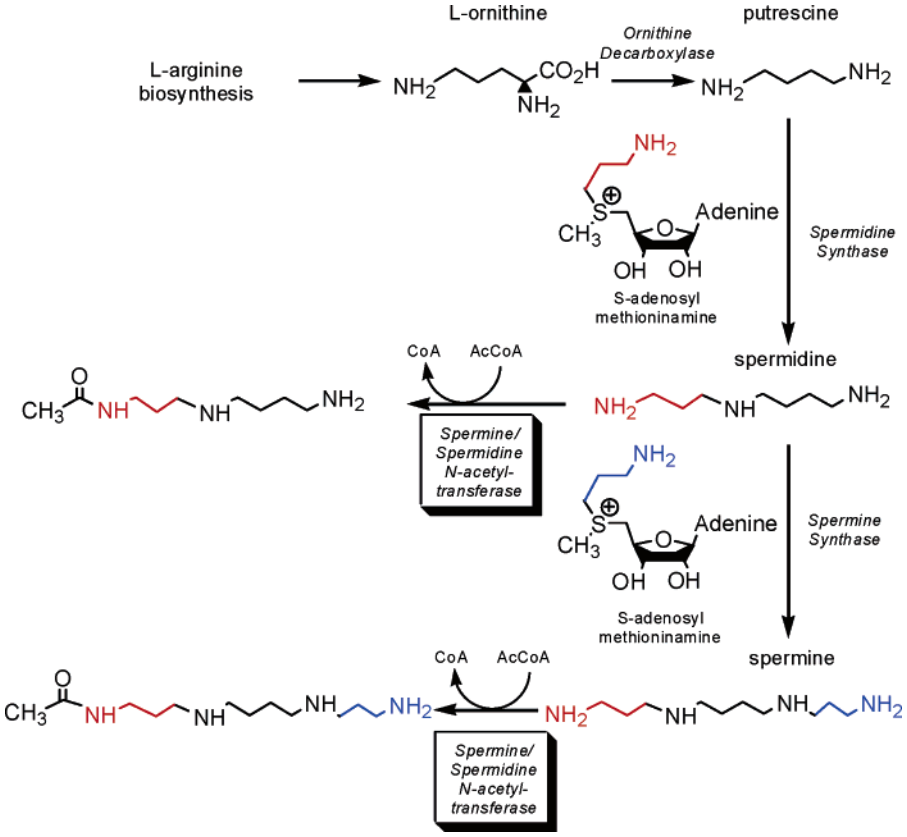

Cloning, Overexpression, and Purification of hSSAT. The open reading frame of the *hSSAT* gene (Swissprot entry P21673) was amplified from the cDNA clone by standard PCR techniques using the oligonucleotides SATF (5′-ATCCCGCTCATATGGCTAAATTCGTGATCCGC-3′) and SATR (5′-ATCCCGCTAAGCTTTCACTCCTCTGTTGC-CAT-3′) containing the underlined *Nde*I and *Hin*dIII restriction sites, respectively. The PCR fragment was cloned into pET-28a(+), and the recombinant hSSAT bearing a thrombin-cleavable N-terminal His_6 tag was expressed in *E. coli* strain BL21(DE3). For shake flask growth, 1 L of LB[1] medium supplemented with kanamycin (35 μg/mL) was inoculated with 10 mL of an overnight culture and incubated at 37 °C. The culture was grown to mid-log phase ($A_{600} \sim 0.8$), cooled to 20 °C, induced with 0.5 mM IPTG, and further incubated overnight at 20 °C.

All purification procedures were carried out at 4 °C. The cells were collected by centrifugation at 6000*g*, resuspended in buffer A [50 mM Tris (pH 7.8) containing 150 mM NaCl] containing protease inhibitors, lysozyme (5 μg/mL), and DNase I (0.1 μg/mL), and stirred for 20 min. The cells were then lysed by sonication, and cell debris was removed by centrifugation at 18000*g* for 30 min. The supernatant was dialyzed against buffer A, loaded onto a Ni-NTA column pre-equilibrated with buffer A, and washed with 10 column volumes of the same buffer. The bound proteins were eluted with a linear 0 to 0.3 M imidazole gradient at a flow rate of 1 mL/min. The active fractions were pooled and concentrated to 5 mL by ultrafiltration. The His_6 tag was then cleaved using thrombin (2 units/mg of protein), and the solution was dialyzed overnight against buffer A containing 2 mM $CaCl_2$ and loaded onto a Superdex S-75 column pre-equilibrated with buffer A. Pure fractions as determined by SDS−PAGE were pooled and concentrated by ultrafiltration.

Protein Estimation. Protein concentrations were estimated by the Bio-Rad protein assay method using bovine serum albumin as a standard.

Synthesis of N^1-Spermine−Acetyl-CoA. Chloroacetyl-CoA was synthesized and purified as described previously (*18*). The N^1-chloroacetylation of spermine by hSSAT was performed using 200 μM ClAcCoA, 200 μM spermine, 50 mM Tris (pH 7.5), and 2 μM hSSAT at room temperature for 1 h. CoA (1 mM) was added, and 200 mM Tris (pH 8.4) was used to increase the pH (to pH 8.2) of the solution that was allowed to stand at 4 °C for 10 h. The pH was adjusted to 2 by the addition of TFA. After removal of the precipitated hSSAT by centrifugation, spermine was separated from CoA and N^1-spermine−acetyl-CoA by HPLC using a Phenomenex Synergi Fusion C18 column (4 μm, 250 mm × 21.2 mm) using a linear 0 to 40% methanol gradient in 0.1% aqueous TFA over 110 min at a rate of 8 mL/min. The retention times of CoA and N^1-spermine−acetyl-CoA were 62 and 68 min, respectively. The identity of the product has been confirmed by mass spectrometry.

Measurement of Enzyme Activity. Reaction rates were measured spectrophotometrically by following the increase in absorbance at 324 nm due to the reaction between the free sulfhydryl group of CoASH, generated by the enzyme-catalyzed polyamine acylating activity, and 4,4′-dithiopyridine. The reaction was monitored continuously on a UVIKON XL spectrophotometer, and enzyme activities were calculated

[1] Abbreviations: IPTG, isopropyl thio-β-D-galactosidase; DTT, dithiothreitol; LB, Luria broth; EDA, ethylenediamine; DET, diethyltriamine.

using a molar absorption coefficient of 19 800 M^{-1} cm^{-1} (*38*). Assay mixtures contained 50 mM Tris (pH 7.5) and 0.2 mM 4,4′-dithiopyridine, in addition to substrates or inhibitors in a volume of 1 mL. Reactions were initiated by the addition of enzyme and followed at room temperature for 1−2 min.

Initial Velocity Experiments. Initial velocity kinetic data were fitted using Sigma Plot 2000. Kinetic constants for AcCoA were determined at fixed, saturating concentrations of spermidine. Kinetic constants for polyamines were determined using fixed, saturating conditions of AcCoA. Individual substrate saturation kinetic data were fitted to eq 1

$$v = (VA)/(A + K) \quad (1)$$

where V is the maximal velocity, A is the substrate concentration, and K is the Michaelis−Menten constant (K_m). Initial velocity patterns were obtained by measuring the initial rate at five concentrations of each substrate. Equation 2 was used to fit the intersecting initial velocity pattern:

$$v = (VAB)/(K_{ia}K_B + K_aB + K_BA + AB) \quad (2)$$

where A and B are the concentrations of the substrates, K_a and K_B are the Michaelis−Menten constants for the substrates, and K_{ia} is the inhibition constant for substrate A.

Bisubstrate Inhibition Patterns. Bisubstrate inhibition patterns were determined by measuring initial velocities at variable concentrations of one reactant (AcCoA or spermidine) with the second reactant concentration fixed (spermidine or AcCoA) and the bisubstrate inhibitor at several concentrations. Equation 3 was used to fit the competitive inhibition data.

$$v = (VA)/[K_a(1 + I/K_{is}) + A] \quad (3)$$

where I is the inhibitor concentration and K_{is} is the slope inhibition constant.

Determination of the True K_i Value. To determine the true K_i value for N^1-spermine-acetyl-CoA, appK_i values were determined from inhibition patterns versus AcCoA at four different concentrations of the nonvaried reactant (spermidine at 27, 40, 56.6, and 100 μM). The appK_i values were plotted against the concentration of spermidine, and the data were fitted to eq 4.

$$\text{app}K_i = K_i(1 + B/K_{ib}) \quad (4)$$

where K_i is the true inhibition constant for N^1-spermine-acetyl-CoA, appK_i is the apparent inhibition constant, B is the concentration of the nonvaried substrate (spermidine), and K_{ib} is the dissociation constant for substrate B.

Dependence of hSSAT Activity on pH. The pH dependence of the kinetic parameters exhibited by hSSAT was determined using AcCoA as the variable substrate. Activity was monitored every 0.3 pH unit from pH 6.7 to 9.1 using the following buffer: HEPES (pH 6.7−7.9) and TAPS (pH 7.6−9.1). The resulting kinetic data were fitted to eq 1 to obtain the kinetic parameters k_{cat} and k_{cat}/K_m. Profiles were generated by plotting the log of k_{cat} or k_{cat}/K_m versus the pH and fitted using the equations

$$\log k_{cat} \text{ or } \log k_{cat}/K_m = \log[C/(1 + [H^+]/K_1 + K_2/[H^+])] \quad (5)$$

where C is the pH-independent plateau value, K_1 is the ionization constant for the acidic group, K_2 is the ionization constant for the basic group, and $[H^+]$ is the hydrogen ion concentration.

Solvent Kinetic Isotope Effects. The solvent kinetic isotope effects on k_{cat} and k_{cat}/K_m were determined by measuring the initial velocities using saturating concentrations of AcCoA while varying the concentration of spermidine in either H_2O or 99% D_2O at pH 8.0. Solvent deuterium kinetic isotope effects were fitted to the following equation:

$$v = (VA)/[KA(1 + F_iE_{V/K}) + A(1 + F_iE_V)] \quad (6)$$

where $E_{V/K}$ and E_V are the isotope effects on $k_{cat}/K_m - 1$ and $k_{cat} - 1$, respectively, and F_i represents the fraction of isotope.

Crystallization and Structure Determination. Protein utilized for crystallization was dialyzed overnight against 20 mM Tris (pH 8.0) containing 1 mM DTT and 0.1 mM EDTA and concentrated to 15 mg/mL by ultrafiltration. Prior to crystallization, N^1-spermine-acetyl-CoA was added to a concentration of 4 mM and the complex was incubated on ice for 2 h. Crystals of hSSAT were grown by hanging drop vapor diffusion at 18 °C; 2 μL of purified protein was combined with 2 μL of the reservoir [3−4 M NaCl, 200 mM K/Na tartrate, 100 mM Tris-HCl (pH 7−8), and 50 mM $MgCl_2$]. Large rectangular crystals grew to their maximal dimensions of 0.5 mm × 0.5 mm × 0.2 mm over 1−3 days. Crystals were briefly soaked in 4 M NaCl, 200 mM K/Na tartrate, 100 mM Tris (pH 7.75), and 50 mM $MgCl_2$ prior to vitrification in liquid nitrogen with the high salt acting as a cryoprotectant. Data were collected utilizing a Rigaku RU300 generator and an R-Axis IV^{++} image plate and scaled using MOSFLM (*19*). Phasing utilized the molecular replacement program AMORE (*20*) and the structure of apo hSSAT (PDB entry 2F5I) (*16*) as a search model. Molecular models were fit to the data using the molecular graphics program COOT (*21*) and refined using REFMAC (*22*). Data and refinement statistics are listed in Table 2. The structural data have been deposited in the Protein Data Bank (PDB entry 2JEV).

RESULTS AND DISCUSSION

Purification and Properties of hSSAT. PCR amplification of the *hSSAT* gene yielded a single fragment of the expected length. Cloning and overexpression of the PCR product resulted in an expressed protein product with an apparent molecular mass, by SDS−PAGE, in agreement with the mass of 20 023 Da deduced from the amino acid sequence. DNA sequencing of the cloned fragment confirmed the absence of any mutations introduced during PCR amplification. The two-step purification procedure yielded a >98% pure protein.

Substrate Specificity of hSSAT. Initial velocities were determined spectrophotometrically, at pH 7.5, at 8−12 different concentrations of each substrate. The data were plotted by nonlinear, least-square curve fitting using Sigmaplot (version 2000). Kinetic constants for acetyl-CoA, determined at a saturating concentration of spermidine, are

Table 1: Kinetic Parameters for Acetyl-Coenzyme A and Polyamines

substrate	K_m (μM)	k_{cat} (min^{-1})	V/K (M^{-1} min^{-1})
acetyl-CoA[a]	3.8 ± 0.2	590 ± 9	155×10^6
spermine[b]	5.7 ± 0.4	155 ± 3	27×10^6
spermidine[b]	22 ± 1	584 ± 9	26×10^6
1,3-diaminopropane[b]	107 ± 4	60 ± 1	56×10^4
diethylenetriamine[b]	194 ± 8	94 ± 2	48×10^4
ethylenediamine[b]	196 ± 30	13 ± 1	66×10^3
putrescine	na[c]		
cadaverene	na[c]		

[a] Measured at a fixed saturating concentration of spermidine. [b] Measured at a fixed saturating concentrations of acetyl-CoA. [c] No detectable activity.

Table 2: Data Collection and Refinement Statistics[a]

Data Collection	
space group	$P4_3$
unit cell dimensions	$a = b = 46.7$ Å, $c = 191.8$ Å
resolution (Å)	50−2.3 (2.42−2.3)
completeness (%)	98.5 (93.9)
redundancy	3.8 (3.3)
$I/\sigma(I)$	20.2 (4.3)
R_{merge} (%)	4.4 (22.6)
Wilson *B*-factor (Å^2)	51.7
Refinement	
resolution (Å)	50−2.3 (2.36−2.3)
R_{factor} (%)	22.4 (27.0)
no. of unique reflections[b]	16978 (1200)/908 (59)
R_{free} (%)	27.5 (37.4)
protein residues fit	A2−A170, B2−B170
no. of atoms	
protein	2784
solvent/ligands	67/130
average *B*-factor (Å^2)	
protein	44.6
solvent/ligands	39.0/68.6
rms deviation	
bonds (Å)	0.011
angles (deg)	1.354

[a] Statistics in parentheses are for the highest-resolution shell. [b] Used in refinement and calculation of R_{factor} and R_{free}.

listed in Table 1. The steady-state kinetic parameters for various polyamines at saturating concentrations of acetyl-CoA are also summarized in Table 1.

From the determined steady-state kinetic parameters, particularly the relative V/K values, acetyl-CoA was the strongly preferred acyl donor (Table 1), while other coenzyme A derivatives either were extremely poor substrates or did not demonstrate any activity (data not shown). hSSAT exhibits somewhat broad specificity with respect to polyamines. Among physiologically relevant substrates, spermidine and spermine were good substrates for hSSAT while their diamine precursor putrescine was not acetylated by hSSAT. The substrate specificity, as evaluated by the V/K values, was the same for both spermine and spermidine. However, both K_m and k_{cat} values were 4-fold higher for spermidine than for spermine. Among the di- and polyamine analogues that were tested, diethylenetriamine (DET) and ethylenediamine (EDA) exhibited significant activity (Table 1). It has previously been reported that acetylation by SSAT occurs on a primary amino group that is linked by a three-carbon unit and that all substrates have the structure R-NH-$(CH_2)_3$-NH_2.The acetylation pattern observed here generally follows the rule described above. However, the acetylation of

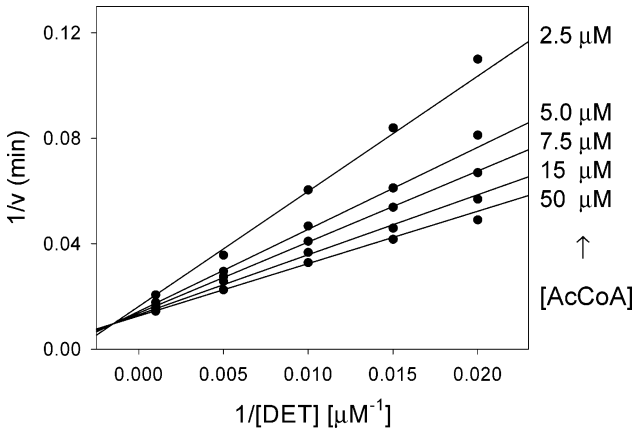

FIGURE 1: Initial velocity pattern. The symbols are experimentally determined values, while the lines are fits of the data to eq 2.

diethylenetriamine and ethylenediamine, but not putrescine or cadaverine (diaminobutane and diaminopentane, respectively), by hSSAT suggests that diamines separated by two methylenes, but not longer alkyl groups, can be acetylated, albeit poorly.

Kinetic Mechanism. The initial velocity pattern was determined using DET and acetyl-CoA at five different concentrations of each substrate. The resultant double-reciprocal plot was intersecting (Figure 1). The intersecting initial velocity plot obtained with DET and acetyl-CoA suggests a sequential kinetic mechanism, where both substrates must be bound to the enzyme for catalysis to occur. The sequential kinetic mechanism appears to be used by all SSATs studied to date (*23*, *24*).

Bisubstrate inhibitors represent a potentially powerful group of compounds that have been synthesized and tested against a number of enzymes that catalyze sequential bireactant reactions, and the detailed theory for predicting the expected patterns of inhibition against the two substrates for various bireactant kinetic mechanisms has recently been reported (*18* and references cited therein). Bisubstrate inhibitors have been extensively used in kinetic and structural studies of the Gcn5-related *N*-acetyltransferase (GNAT) superfamily, to which the SSATs belong (*25*−*29*).

N^1-Spermine-acetyl-CoA exhibited linear, competitive inhibition versus both acetyl-CoA (Figure 2A) and spermidine (data not shown). These data are compatible with a random mechanism in which either of the substrates can bind to the free enzyme. Kinetic analyses of *Bacillus subtilis* (*23*) and rat liver (*24*) SSATs have previously been reported. The rat liver SSAT was reported to follow an ordered sequential mechanism, where polyamine binds first followed by acetyl-CoA (*24*), while the *B. subtilis* enzyme was reported to use a random mechanism (*23*). It is interesting to note that rat liver SSAT (*24*) and hSSAT are 97% identical in sequence yet apparently differ in their kinetic mechanism.

When the apparent K_i value versus acetyl-CoA of the N^1-spermine-acetyl-CoA was determined at several concentrations of spermidine, the apparent K_i value decreased as the spermidine concentration decreased, as expected for an inhibitor that binds to both substrate-binding sites (Figure 2B). These data allowed the determination of the true K_i value for the binding of the bisubstrate to the free enzyme by extrapolation to [spermidine] = 0, yielding a K_i value of 6 ± 1 nM.

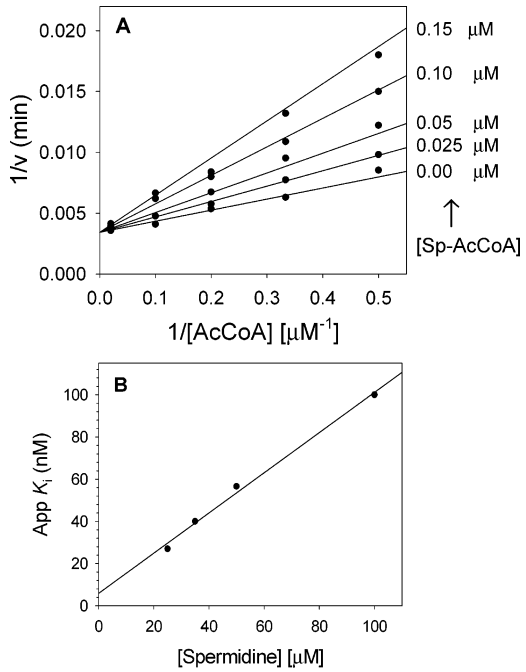

FIGURE 2: Bisubstrate inhibition of hSSAT. (A) Inhibition pattern of spermine-AcCoA vs AcCoA at a fixed spermidine concentration of 50 μM. (B) Linear dependence of appK_i values at various concentrations of spermidine. Symbols are experimentally determined K_i values of spermine-AcCoA vs AcCoA at different fixed spermidine concentrations, while the line is the fit of the data to eq 4.

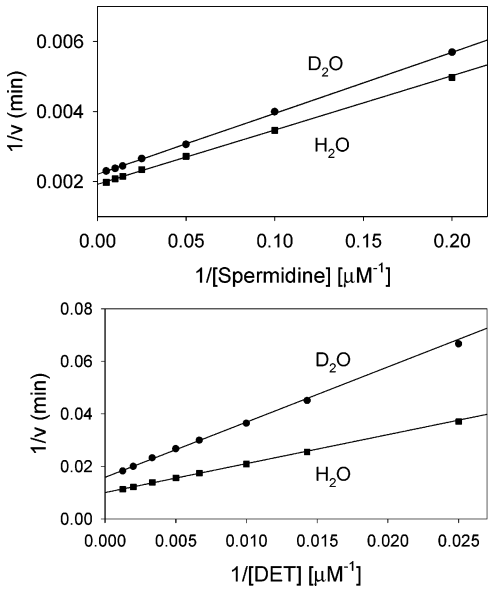

FIGURE 3: Solvent kinetic isotope effect for hSSAT. The symbols are experimentally determined values in H_2O (■) or 99% D_2O (●); the lines are fits of the data to eq 6. Spermidine and DET were variable substrates at a fixed, saturating concentration of AcCoA.

Studies of solvent kinetic isotope effects can be a useful tool in the determination of rate-limiting chemical steps and the kinetic mechanism, especially in distinguishing between steady-state random and rapid equilibrium random mechanisms. In a rapid equilibrium random kinetic mechanism, the rates of substrate binding and product dissociation are very fast relative to the catalytic step, and equivalent isotope effects must be observed on V and V/K. This is not a requirement for the steady-state random mechanism. Solvent kinetic isotope effects were determined at pH 8.0, in both H_2O and 99% D_2O, a region where small changes in pH(D) did not have any effect on the kinetic parameters (see below). Reactions were performed at fixed, saturating concentrations of acetyl-CoA and at varying polyamine concentrations. Two different polyamines, spermidine and DET, exhibiting relatively low and high K_m values, respectively, were used. The solvent kinetic isotope effects on V were 1.15 ± 0.01 and 1.59 ± 0.02 using spermidine and DET, respectively (Figure 3). The solvent kinetic isotope effects on V/K were 1.12 ± 0.03 and 1.91 ± 0.06 for spermidine and DET, respectively (Figure 3).

The very low value of the solvent kinetic isotope effects on V/K determined with spermidine suggests that spermidine is kinetically "sticky", and that no slow, solvent isotopically sensitive step occurs between spermidine binding and the first irreversible step, generally assumed to be the release of first product. The larger value of the solvent kinetic isotope effect on V/K obtained using DET likely reflects the lower commitment factor of this poorer substrate. The larger values of the solvent kinetic isotope effects on V, which includes steps from the precatalytic ternary complex through final product release, may reflect the effects of solvent isotopic substitution on the chemical step, the release of products, or the conformational changes that allow this to occur. The magnitude of the solvent kinetic isotope effects and the inequality of ^{D_2O}V and $^{D_2O}V/K$ argue against a rapid equilibrium random mechanism in which the chemical step is rate-limiting.

Structure of hSSAT with Bound N^1-Spermine-Acetyl-CoA. To confirm that the bisubstrate interacted in a kinetically relevant fashion with hSSAT, its three-dimensional structure bound to hSSAT was pursued. Initial crystallization searches to produce a hSSAT−bisubstrate complex utilized commercial screens and vapor diffusion under oil. These screens yielded a single crystal form ($P6_2$, $a = b = 66.9$ Å, $c = 78.6$ Å) similar to that reported by Bewley et al. [PDB entries 2B3V and 2B58 (*17*)]. Examination of electron density maps indicated a symmetric dimer with CoA bound in each active site, which presumably is copurified with the enzyme, and no density for the bisubstrate (data not shown). Presumably, this crystal form is not compatible with the structural conformation required for binding of the bisubstrate. Narrower crystallization trials were initiated around those used previously to crystallize hSSAT in other forms [PDB entries 2F5I and 2BEI (*16*)]. New crystals were obtained under high-salt conditions similar to those used to crystallize hSSAT in an apo form. Examination of electron density maps clearly indicates electron density for the CoA and polyamine functions of the bisubstrate (Figure 4). The *c*-axis of this crystal form with bound bisubstrate increases by 10 Å over that of the apo structure (191.8 and 180.5 Å, respectively), while the *a*- and *b*-axes remain unchanged. A crystal contact in the direction of the *c*-axis positions two crystallographically related CoA binding sites in the proximity of the *c*-axis and must therefore expand to accommodate the adenosine functionality of the bound bisubstrate inhibitor. Interestingly, there are only minor structural rearrangements upon binding the bisubstrate analogue compared to the apoenzyme form (rmsd of 0.43 Å, over 333 common Cα atoms). The largest movements were limited to two regions: (1) the pyrophosphate binding loop (β4−α3), specifically the side chain of

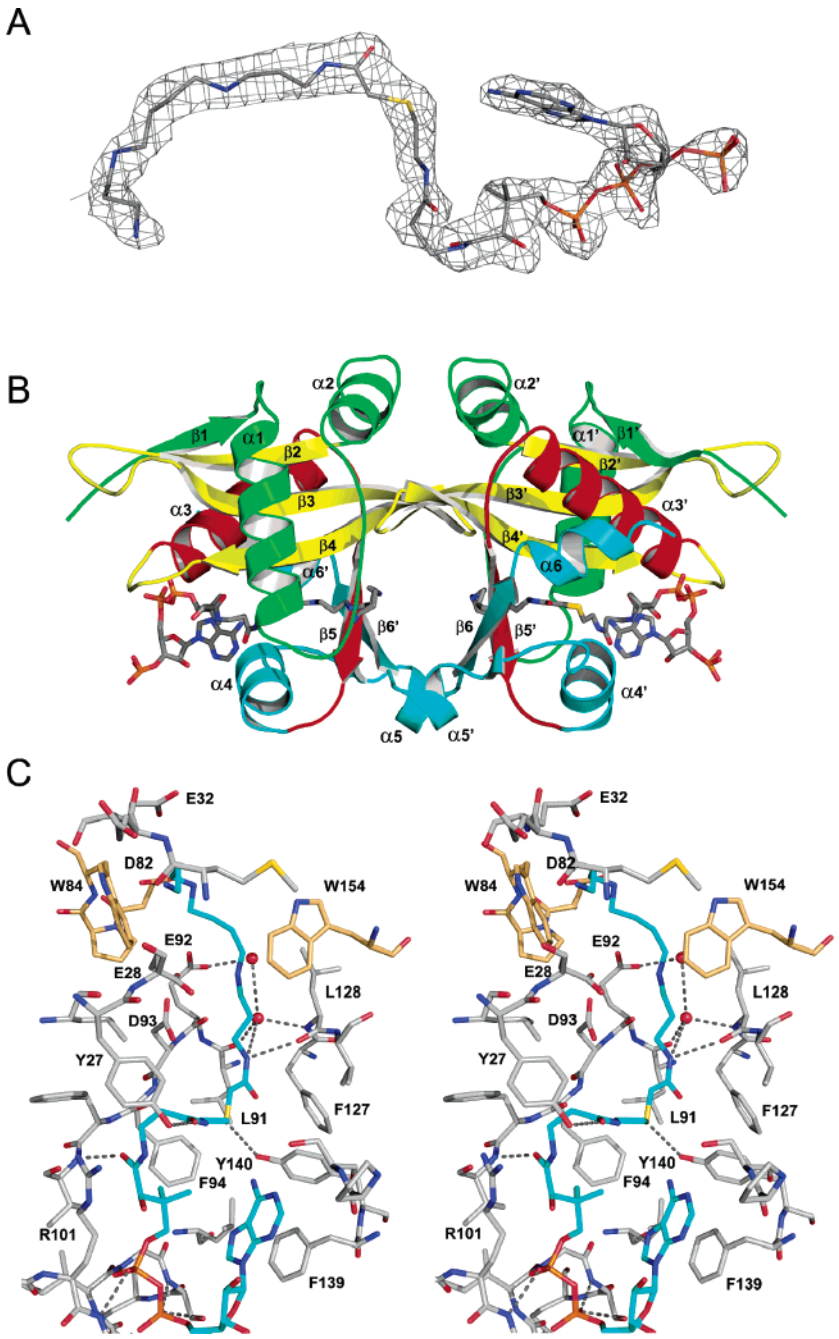

FIGURE 4: Structure of hSSAT witha bisubstrate analogue. (A) Final $2F_o - F_c$ electron density for the bisubstrate analogue contoured at 1σ. (B) Ribbon diagram of the hSSAT dimer colored according to the color scheme for conserved GNAT secondary structure in Vetting et al. (*30*) [green for β1, α1, and α2, yellow for β2, β3, and β4, red for α3 and β5, and cyan for α4, β5, (α5), β6, and (α7)]. The bisubstrate analogue is displayed as sticks, colored by atom type. (C) Stereodiagram depicting residues within 5 Å of the bisubstrate analogue colored by atom type. Residues from the opposing subunit are colored with tan carbons, while the bisubstrate is colored with cyan carbons. Potential hydrogen bonds are displayed as gray dotted lines.

Arg101 which moves to optimize its van der Waals contacts with the panothenic acid moiety of CoA, and (2) the α1−α2 loop which provides contacts with both CoA and the C8−N12 portion of spermine. Specifically, the side chain of Tyr27 changes rotamers to maximize its interactions with the β-alanine moiety of CoA, and the α1−α2 loop changes conformation to maximize the electrostatic interactions of Glu32 and Glu28 with N12 of spermine.

There may be some limitations to the interpretation of the structure of the bisubstrate complex in this crystal form, which the authors consider a conformationally restricted apo structure interacting with the bisubstrate. There is some indication that the occupancy of the bisubstrate is <1.0. The average *B*-factor for the bisubstrate is 20−30 Å^2 larger than those for the surrounding protein atoms, and there is residual electron density for the side chain of Tyr27 in its "apo" rotamer. In addition, α4 remains in its apo position, instead of moving closer to and interacting fully with the pantothenoate portion of CoA, which was demonstrated in an hSSAT−AcCoA complex (PDB entry 2B3V) (*17*) and in accordance with the position of α4 in numerous other GNAT structures (*30*). Instead, the adenosine moiety, which normally interacts with surface residues, is wedged between α4 and the pantothenate, with the adenine stacking face to face

against Phe139. However, the structure determined here provides interesting structural details. First, the structure demonstrates that the bisubstrate analogue can occupy both the CoA and the polyamine binding site, as suggested by the competitive inhibition pattern of the bisubstrate against both CoA and polyamine substrates. Second, the bisubstrate structure can be compared to the structure of hSSAT with the inhibitor N^1,N^{11}-bis(ethyl)norspermine [BE-3-3-3, PDB entry 2B4B (*17*)], shedding more light on the polyamine binding site and potential residues involved in the acid/base chemistry. The polyamine functionality of the bisubstrate (Figure 4C) and BE-3-3-3 both interact through van der Waals contacts with L128 and the side chains of W154* and W84* (residues with an asterisk are from the opposing monomer of the dimer.) Differences are observed in the loop from which W84* originates as it is in an alternate conformation in the BE-3-3-3 complex. The C9-N11-ethyl moieties of BE-3-3-3 are positioned differently than the corresponding terminal atoms of the bisubstrate such that BE-3-3-3 interacts with the edge instead of the face of side chain W84* (Figure S1 of the Supporting Information). There are five electronegative side chains that line the pocket (E28, E32, D82*, E92, and D93) and are adjacent to either N4, N9, or N12 of spermine. Interestingly, none interact directly, or through any water molecules visualized at this resolution, similar to the mode of interaction of hSSAT observed with BE-3-3-3. This suggests that polyamines may interact, or are attracted to, the active site by long-range electrostatics. However, they are not restrained by hydrogen bonding to such acidic residues and are instead free to move within the active site cavity to optimize van der Waals interactions.

BE-3-3-3 appears not to penetrate the active site as deeply as the hSSAT bisubstrate complex would suggest, with the N1-ethyl moiety of BE-3-3-3 overlaying with C2 and C3 of spermine and the N1 moiety of BE-3-3-3 positioned close to N4 of the spermine moiety. In the bisubstrate complex, N1 of spermine is hydrogen bonded to the carbonyl oxygen of Leu128 of strand β5, similar to the interaction observed in many other GNAT family members, and therefore, its position is unlikely to be disrupted due to the bisubstrate linkage (Figure 4C). In the hSSAT−AcCoA complex (*17*), the thioester carbonyl is hydrogen bonded to the backbone amide of Phe94 on β4. This hydrogen bond is broken in the bisubstrate complex, with the carbonyl group now interacting with the side chain hydroxyl of Tyr140. It is not clear if this interaction is a model for a product complex or is a strained interaction due to the covalent bond between CoA and N^1-acetylspermine of the bisubstrate.

To examine which groups observed in the active site may participate in the acid and/or base catalysis of the reaction, the pH dependence of the reaction was determined. The k_{cat}−pH profile of the acetyl transfer reaction by hSSAT was bell-shaped, with unitary limiting slopes (+1, −1) at the pH extremes (Figure 5), suggesting the involvement of two groups whose ionization is critical for catalytic activity. The pH dependence of k_{cat} suggests that the deprotonation of a single group exhibiting a pK value of 8.87 ± 0.05 and the protonation of a single group exhibiting a pK value of 7.27 ± 0.04 cause a loss of catalytic activity (Figure 5). A possible role for the group exhibiting a pK value of 8.87 is to function as a general acid by donating a proton to the sulfur of coenzyme A during the collapse of the tetrahedral intermediate. Various hSSAT structures, including the bisubstrate complex presented here, suggest that the side chain phenolic OH group of Tyr140 is in position to protonate the sulfhydryl of CoA (*17*). In addition, the substitution of Tyr140 with a phenylalanine reduced the activity to <5% (*17*). The group that exhibits a pK value of 7.27 is most likely an enzyme group that acts as a general base to promote catalysis via abstraction of a proton from the amino group of the polyamine that is being acetylated. Bewley et al. (*17*) proposed that Glu28 might act as the general base; however, its mutation to a glutamine reduced activity by only 55% with a 3-fold increase in the K_m value of spermidine (*31*). One would expect a significantly larger decrease in the catalytic activity if Glu28 functioned in this chemical role, and in the bisubstrate complex, Glu28 is not well positioned to accept protons from the amine of substrate. Instead, the bisubstrate structure suggests Glu92, through one or more waters, is the terminal proton acceptor and responsible for acidic pK value of 7.27 that is observed. A water molecule, positioned in the splay between β4 and β5, and hydrogen bonded to the backbone carbonyl of Glu92 and the amide nitrogen of Leu128 is a conserved feature of GNAT ternary complexes determined to date and is stereochemically well positioned to accept the proton from the substrate and pass it on to an adjoining water or directly to Glu92.

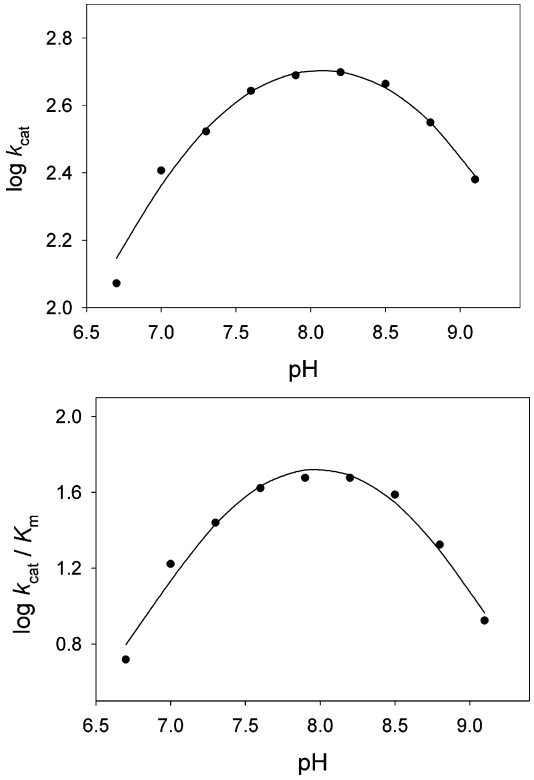

FIGURE 5: pH−activity profile of hSSAT. The symbols are experimentally determined values, while the smooth line is a fit of the data to eq 5.

We therefore propose a model for the reaction catalyzed by hSSAT that includes this acid/base assistance (Figure 6). Either of the substrates can bind to the free enzyme, and once the ternary complex is formed, nucleophilic attack on the carbonyl of the thioester generates the zwitterionic, tetrahedral intermediate. On the basis of our pH studies, we invoke the participation of a general acid (Tyr140) to assist in protonating the sulfur of the coenzyme A and a general

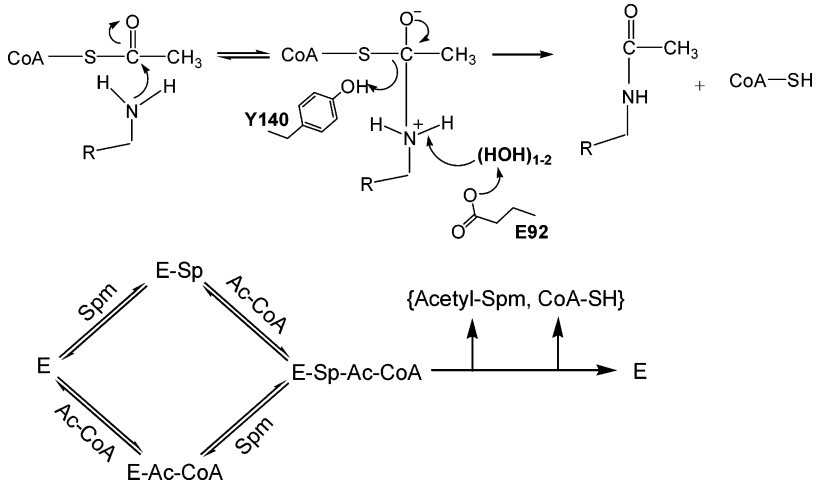

FIGURE 6: Proposed chemical and kinetic mechanism for acetyl transfer activity by hSSAT.

base (Glu92) to deprotonate either the positively charged N1-amine of the substrate or the zwitterionic intermediate. Similar mechanisms involving catalysis by promoting the appropriate decomposition of a similar tetrahedral intermediate have been proposed for several GNATs (*32*−*36*). The chemical steps portrayed in Figure 6 are not likely to be rate-determining on the basis of the magnitude of the solvent kinetic isotope effects. The purified and crystallized apoenzyme contains bound CoA, suggesting that CoA is copurified with the enzyme and is thus bound tightly. Thus, CoA dissociation is likely to be the rate-limiting step, as observed for other *N*-acetyltransferases (*32*, *37*).

SUPPORTING INFORMATION AVAILABLE

Three figures showing the superposition of the hSSAT bisubstrate analogue complex and the hSSAT−BE-3-3-3 complex (PDB entry 2B4B) (Figure S1), structures of the bisubstrate inhibitor, BE-3-3-3, and other polyamines used in the study (Figure S2), and the mass spectrum of the synthesized bisubstrate analogue (Figure S3). This material is available free of charge via the Internet at http://pubs.acs.org.

REFERENCES

1. Casero, R. A., Jr., Celano, P., Ervin, S. J., Applegren, N. B., Wiest, L., and Pegg, A. E. (1991) Isolation and characterization of a cDNA clone that codes for human spermidine/spermine N1-acetyltransferase, *J. Biol. Chem. 266*, 810−814.
2. Pegg, A. E. (1986) Recent advances in the biochemistry of polyamines in eukaryotes, *Biochem. J. 234*, 249−262.
3. Pegg, A. E. (1998) Polyamine metabolism and its importance in neoplastic growth and a target for chemotherapy, *Cancer Res. 48*, 759−774.
4. Moinard, C., Cynober, L., and de Bandt, J. (2005) Polyamines: Metabolism and implications in human diseases, *Clin. Nutr. 24*, 184−197.
5. Morrison, L. D., and Kish, S. J. (1995) Brain polyamine levels are altered in Alzheimer's disease, *Neurosci. Lett. 197*, 5−8.
6. Russell, D. H., Rosenblum, M. G., Beckerman, R. C., Durie, B. G., Taussig, L. M., and Barnett, D. R. (1979) Altered polyamine metabolism in cystic fibrosis, *Pediatr. Res. 13*, 1137−1140.
7. Rosenblum, M. G., Durie, B. G., Beckerman, R. C., Taussig, L. M., and Russell, D. H. (1978) Cystic fibrosis: Decreased conjugation and excretion of [^{14}C]spermidine, *Science 200*, 1496−1497.
8. Russell, D. H. (1971) Increased polyamine concentrations in the urine of human cancer patients, *Nat. New Biol. 233*, 144−145.
9. Russell, D. H. (1972) Effects of methotrexate and cytosine arabinoside on polyamine metabolism in a mouse L1210 leukemia, *Cancer Res. 32*, 2459−2462.
10. Janne, J., Poso, H., and Raina, A. (1978) Polyamines in rapid growth and cancer, *Biochim. Biophys. Acta 473*, 241−293.
11. Casero, R. A., Jr., Ervin, S. J., Celano, P., Baylin, S. B., and Bergeron, R. J. (1989) Differential response to treatment with the bis(ethyl)polyamine analogues between human small cell lung carcinoma and undifferentiated large cell lung carcinoma in culture, *Cancer Res. 49*, 639−643.
12. Bernacki, R. J., Bergeron, R. J., and Porter, C. W. (1992) Antitumor activity of N,N′-bis(ethyl) spermine homologues against human MALME-3 melanoma xenografts, *Cancer Res. 52*, 2424−2430.
13. Seiler, N. (2004) Catabolism of polyamines, *Amino Acids 26*, 217−233.
14. Casero, R. A., Jr., and Pegg, A. E. (1993) Spermidine/spermine N^1-acetyltransferase-the turning point in polyamine metabolism, *FASEB J. 7*, 653−661.
15. Libby, P. R., Ganis, B., Bergeron, R. J., and Porter, C. W. (1991) Characterization of human spermidine/spermine N^1-acetyltransferase purified from cultured melanoma cells, *Arch. Biochem. Biophys. 284*, 238−244.
16. Zhu, Y. Q., Zhu, D. Y., Yin, L., Zhang, Y., Vonrhein, C., and Wang, D. C. (2006) Crystal structure of human spermidine/spermine N1-acetyltransferase (hSSAT): The first structure of a new sequence family of transferase homologous superfamily, *Proteins 63*, 1127−1131.
17. Bewley, M. C., Graziano, V., Jiang, J., Matz, E., Studier, F. W., Pegg, A. E., Coleman, C. S., and Flanagan, J. M. (2006) Structures of wild-type and mutant human spermidine/spermine N^1-acetyltransferase, a potential therapeutic drug target, *Proc. Natl. Acad. Sci. U.S.A. 103*, 2063−2068.
18. Yu, M., Magalhães, M. L., Cook, P. F., and Blanchard, J. S. (2006) Bisubstrate Inhibition: Theory and Application to *N*-acetyltransferases, *Biochemistry 45*, 14788−14794.
19. Leslie, A. G. (2006) The integration of macromolecular diffraction data, *Acta Crystallogr. D62*, 48−57.
20. Navaza, J. (1994) An automated package for molecular replacement. *Acta Crystallogr. A50*, 157−163.
21. Emsley, P., and Cowtan, K. (2004) Coot: Model-building tools for molecular graphics. *Acta Crystallogr. D60*, 2126−2132.
22. Murshudov, G. N., Vagin, A. A., and Dodson, E. J. (1997) Refinement of macromolecular structures by the maximum-likelihood method, *Acta Crystallogr. D53*, 240−255.
23. Woolridge, D. P., Martinez, J. D., Stringer, D. E., and Gerner, E. W. (1999) Characterization of a novel spermidine/spermine acetyltransferase, BltD, from *Bacillus subtilis*, *Biochem. J. 340*, 753−758.
24. Della Ragione, F., and Pegg, A. E. (1983) Studies of the specificity and kinetics of rat liver spermidine/spermine N^1-acetyltransferase, *Biochem. J. 213*, 701−706.
25. Williams, J. W., and Northrop, D. B. (1979) Synthesis of a tight-binding, multisubstrate analog inhibitor of gentamicin acetyltransferase I, *J. Antibiot. 32*, 1147−1154.

26. Gao, F., Yan, X., Baettig, O. M., Berghuis, A. M., and Auclair, K. (2005) Regio- and Chemoselective 6′-N-derivatization of Aminoglycosides: Bisubstrate Inhibitors as Probes to Study Aminoglycoside 6′-N-Acetyltransferases, *Angew. Chem., Int. Ed. 44*, 6859−6862.
27. Khalil, E. M., and Cole, P. A. (1998) A Potent Inhibitor of the Melatonin Rhythm Enzyme, *J. Am. Chem. Soc. 120*, 6195−6196.
28. Hickman, A. B., Namboodiri, M. A. A., Klein, D. C., and Dyda, F. (1999) The Structural Basis of Ordered Substrate Binding by Serotonin N-Acetyltransferse: Enzyme Complex at 1.8 Å Resolution with a Bisubstrate Analog, *Cell 97*, 361−369.
29. Poux, A. N., Cebrat, M., Kim, C. M., Cole, P. A., and Marmorstein, R. (2002) Structure of the GCN5 Histone Acetyltransferase Bound to a Bisubstrate Inhibitor, *Proc. Natl. Acad. Sci. U.S.A. 99*, 14065−14070.
30. Vetting, M. W., de Carvalho, L. P. S., Yu, M., Hegde, S. S., Magnet, S., Roderick, S. L., and Blanchard, J. S. (2005) Structure and functions of the GNAT superfamily of acetyltransferases, *Arch. Biochem. Biophys. 433*, 212−226.
31. Coleman, C. S., Huang, H., and Pegg, A. E. (1995) Role of the carboxyl terminal MATEE sequence of spermidine/spermine N1-acetyltransferase in the activity and stabilization by the polyamine analog N1,N12-bis(ethyl)spermine, *Biochemistry 34*, 13423−13430.
32. Magnet, S., Lambert, T., Courvalin, P., and Blanchard, J. S. (2001) Kinetic and mutagenic characterization of the chromosomally encoded *Salmonella enterica* AAC(6′)-Iy aminoglycoside N-acetyltransferase, *Biochemistry 40*, 3700−3709.
33. Vetting, M. W., Hegde, S. S., Javid-Majd, F., Blanchard, J. S., and Roderick, S. L. (2002) Aminoglycoside 2′-N-acetyltransferase from *Mycobacterium tuberculosis* in complex with coenzyme A and aminoglycoside substrates, *Nat. Struct. Biol. 9*, 653−658.
34. Magalhaes, M. L., and Blanchard, J. S. (2005) The kinetic mechanism of AAC3-IV aminoglycoside acetyltransferase from *Escherichia coli*, *Biochemistry 44*, 16275−16283.
35. Hegde, S. S., and Blanchard, J. S. (2003) Kinetic and mechanistic characterization of recombinant *Lactobacillus viridescens* FemX (UDP-N-acetylmuramoyl pentapeptide-lysine N^6-alanyltransferase), *J. Biol. Chem. 278*, 22861−22867.
36. Hickman, A. B., Klein, D. C., and Dyda, F. (1999) Melatonin biosynthesis: The structure of serotonin N-acetyltransferase at 2.5 Å resolution suggests a catalytic mechanism, *Mol. Cell 3*, 23−32.
37. Vetting, M. W., Magnet, S., Nieves, E., Roderick, S. L., and Blanchard, J. S. (2004) A bacterial acetyltransferase capable of regioselective N-acetylation of antibiotics and histones, *Chem. Biol. 11*, 565−573.
38. Grassetti, D. R., and Murray, J. F., Jr. (1967) Determination of Sulfhydryl Groups with 2,2′- or 4,4′-Dithiopyridine. *Arch. Biochem. Biophys. 119*, 41−49.

BI700256Z